nature COMMUNICATIONS

ARTICLE

Received 6 Jul 2015 | Accepted 10 Dec 2015 | Published 27 Jan 2016

DOI: 10.1038/ncomms10455 OPEN

Nanoelectronic primary thermometry below 4 mK

D.I. Bradley[1], R.E. George[1], D. Gunnarsson[2], R.P. Haley[1], H. Heikkinen[2], Yu. A. Pashkin[1,3], J. Penttilä[4], J.R. Prance[1], M. Prunnila[2], L. Roschier[3] & M. Sarsby[1]

Cooling nanoelectronic structures to millikelvin temperatures presents extreme challenges in maintaining thermal contact between the electrons in the device and an external cold bath. It is typically found that when nanoscale devices are cooled to ~10 mK the electrons are significantly overheated. Here we report the cooling of electrons in nanoelectronic Coulomb blockade thermometers below 4 mK. The low operating temperature is attributed to an optimized design that incorporates cooling fins with a high electron–phonon coupling and on-chip electronic filters, combined with low-noise electronic measurements. By immersing a Coulomb blockade thermometer in the ^{3}He/^{4}He refrigerant of a dilution refrigerator, we measure a lowest electron temperature of 3.7 mK and a trend to a saturated electron temperature approaching 3 mK. This work demonstrates how nanoelectronic samples can be cooled further into the low-millikelvin range.

[1] Department of Physics, Lancaster University, Bailrigg, Lancaster LA1 4YB, UK. [2] VTT Technical Research Centre of Finland, P.O. Box 1000, 02044 VTT Espoo, Finland. [3] Lebedev Physical Institute, Moscow 119991, Russia. [4] Aivon Oy, Valimotie 13A, 00380 Helsinki, Finland. Correspondence and requests for materials should be addressed to J.R.P. (email: j.prance@lancaster.ac.uk) or to M.P. (email: mika.prunnila@vtt.fi) or to L.R. (email: leif.roschier@iki.fi).

Understanding how to obtain and measure electron temperatures approaching 1 mK has the potential to open a new regime for studying nanoelectronics and pave the way towards pioneering sub-millikelvin techniques[1]. This would benefit numerous areas of activity; for example, investigations of the fractional quantum Hall effect in two-dimensional electron gases[2,3] and solid-state quantum technologies including superconducting and semiconducting qubits[4,5]. To access these temperatures one must minimize parasitic heating and internal Joule heating, and maximize the coupling to cold contact wires and phonons in the host lattice, all the while overcoming the decrease in electron–phonon coupling and electrical heat conduction as temperatures drop[6].

Here we study Coulomb blockade thermometers (CBTs) that have been designed to operate significantly below 10 mK and demonstrate cooling of electrons in a nanoelectronic device to below 4 mK. A CBT consists of an array of Coulomb-blockaded metallic islands connected by tunnel junctions. The conductance of the array is temperature dependent, due to the balance between thermal excitations and an electrostatic barrier to single electron tunnelling across the islands[7,8]. CBTs typically function over a decade of temperature and have previously been demonstrated to work at temperatures as low as 7.5 mK (refs 9,10). Perhaps most importantly, they can be viewed as a primary thermometer of their internal electron temperature. We have used CBTs as a diagnostic tool to quantify and optimize the thermal environment of a nanoelectronic device and to unambiguously determine the local electron temperature. In the future, similar CBTs could be used to probe the electron temperature of nearby samples with thermal contact provided by direct electrical connections. Furthermore, the techniques that are used to cool the CBTs can be used to cool other nanoelectronic samples.

Results

Structure of the thermometer devices. The structure of the CBTs studied here is shown in Fig. 1. Devices are fabricated using an *ex situ* tunnel junction process[11], which provides excellent tunnel junction uniformity[12], and has also been used to fabricate superconducting qubits[13] (see Methods for details). Efficient thermal coupling between electrons and phonons in the metallic islands of the CBT is critical for reaching low electron temperatures[14,15]. The electron–phonon heat flow P_{ep} is described by the material-dependent electron–phonon coupling constant Σ and the volume of the metallic island Ω,

$$P_{ep} = \Sigma\Omega\left(T_e^5 - T_p^5\right), \quad (1)$$

where T_e is the electron temperature and T_p is the phonon temperature[16]. To minimize T_e, the island volume should be large and the material chosen to maximize Σ. We use electroplated Au on top of the CBT islands to increase their volume to nominal $5 \times 205 \times 38.5\,\mu m^3$ (see Methods for details). The effective electron–phonon coupling in these islands, with a relatively large volume and a high coupling constant[17] in Au $\Sigma = 2.4 \times 10^9\,WK^{-5}\,m^{-3}$, is estimated to be more than two orders of magnitude larger than in previous CBTs fabricated using the *ex situ* junction process[18].

In addition to efficient thermalization of the CBT itself, it is important to cool the incoming leads through robust thermal anchoring and heavy electromagnetic filtering[19]. We improve the chain of thermalization and filtering by including on-chip resistive meander structures in line with all electrical contacts. These form a distributed resistive-capacitive chain with a cutoff frequency ≈ 40 MHz. Similar filters based on a large area capacitor and tunnel junctions in series have previously been incorporated in a CBT[18].

CBT characteristics above 7 mK. Figure 2 shows the behaviour of a CBT fabricated using the process described above, focusing on temperatures between 7 and 80 mK. The sensor is measured in both a commercial cryogen-free dilution refrigerator (Bluefors Cryogenics LD250) with a base temperature ≈ 7 mK and in a custom dilution refrigerator manufactured at Lancaster University[20] with a base temperature ≈ 2.5 mK. The conductance of the CBT is measured in a current-driven four-wire configuration, with the drive current and voltage amplification provided by an Aivon PA10 amplifier. A small AC excitation (typically $5\,pA \le I_{AC} \le 100\,pA$) is added to the DC bias I_{DC}, allowing the differential conductance G to be measured with a lock-in amplifier.

In both refrigerators, the CBT is in a vacuum and housed in a gold-plated copper package (Aivon SH-1) that is attached to the mixing chamber plate. The package includes RC filters with a cutoff frequency ≈ 300 kHz. Electrical contacts to the CBT are thermalized in additional cold *RC* filters potted in Eccosorb CR

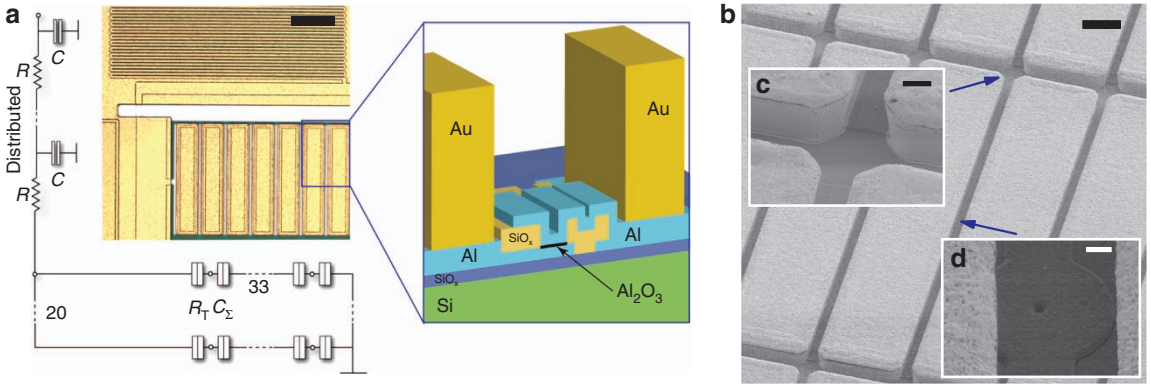

Figure 1 | Details of the CBT device structure. (**a**) Optical micrograph of the CBT with equivalent circuit diagram and schematic cross-section of the structure. Scale bar on the optical micrograph, 10 μm. The CBT is formed of 32×20 metallic islands of capacitance C_Σ connected in an array by tunnel junctions of resistance R_T, as shown in the circuit diagram. Connection to the array is made via on-chip *RC* filters comprising a meandering electrode sandwiched between large-area grounded metal films, separated by 250 nm SiO_x. Each filter has a distributed resistance $R \approx 500\,\Omega$ and capacitance $C \approx 10$ pF. The schematic cross-section shows one Al_2O_3 tunnel junction connecting two Al islands, with Au thermalization blocks on top of each. (**b**) Scanning electron microscopic (SEM) image showing Au thermalization blocks. Scale bar, 20 μm. (**c**) The sidewalls of four adjacent Au blocks. Scale bar, 4 μm. (**d**) One tunnel junction connecting two adjacent blocks. Scale bar, 1 μm.

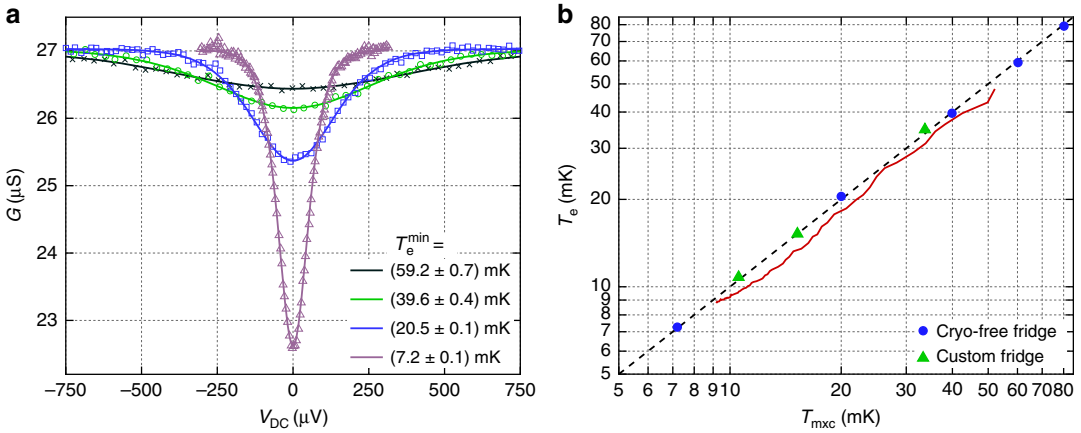

Figure 2 | CBT behaviour between 80 and 7 mK in two dilution refrigerators. (**a**) CBT conductance G versus measured bias voltage V_{DC} at four temperatures. Symbols show measured values and lines show best fits to the calculated ideal conductance. The warmest measurements (crosses, circles and squares) are fitted simultaneously to calibrate the sensor, giving $C_\Sigma = 236.6$ fF and $R_T = 22.42\,k\Omega$. The coldest measurement (triangles) is fitted using this calibration. The minimum electron temperatures T_e^{min} are in close agreement with the refrigerator temperature measured by a RuO_2 thermometer: 59.9, 40.1, 20.0 and 7.2 mK respectively. The uncertainties on T_e^{min} are calculated from uncertainties in the fitted parameters. (**b**) CBT electron temperature T_e versus refrigerator temperature T_{mxc}. Symbols show T_e^{min} from fits to conductance dips measured in the cryogen-free refrigerator (circles) and the custom refrigerator (triangles). Error bars are within the symbols. The solid curve shows T_e determined by monitoring the conductance G_0 (at $V_{DC} = 0$) as the cryo-free fridge cools over 35 min from 52 to 9 mK, showing that the CBT has a stronger thermal link to the refrigerator than the RuO_2 thermometer, leading to the thermal lag ($T_{mxc} \geq T_e$) during this time. The dashed line shows $T_e = T_{mxc}$.

124 (Aivon Therma), which are also attached to the mixing chamber plate. The filters have a cutoff frequency ≈ 15 kHz.

As shown in Fig. 2a, the CBT conductance dips around zero bias and the dip becomes deeper and narrower at lower temperatures. Its full-width at half maximum is related to temperature by $V_{1/2} \approx 5.439 N k_B T/e$, where N is the number of tunnel junctions in series[7]. This result does not account for self-heating in the sensor and so is only applicable when $T_e = T_p \equiv T$. A more practical parameter to determine temperature is the zero-bias conductance G_0, which has an approximate analytic relation to temperature[21]

$$G_0 \approx G_T\left(1 - 1/6u_N - 1/60u_N^2 + 1/630u_N^3\right), \qquad (2)$$

where $u_N \equiv E_C/k_B T$ is the dimensionless inverse temperature, $E_C \equiv [(N-1)/N]e^2/C_\Sigma$ is the charging energy of the system, C_Σ is the total capacitance of each island and G_T is the asymptotic conductance. When $u_N < 2.5$, the temperature measurement error is $< 2.5\%$ (ref. 15). Thus, if C_Σ and G_T are known, it is possible to determine T by measuring only G_0. The most complete method to determine temperature is using a full tunnelling model to calculate $G(V_{DC})$ numerically[7]. We use this last approach to find C_Σ and G_T for the device, and these parameters are then used to find the temperature from subsequent measurements.

Numerical calculations of conductance are made using an algorithm derived from the free, open-source library pyCBT (see Methods for further details). In addition, we account for overheating in the sensor by predicting the electron temperature T_e in the islands using a model for the heat flow P into each island,

$$P = \frac{V_{DC}^2}{R_T} - \Sigma\Omega\left(T_e^5 - T_p^5\right) + P_0, \qquad (3)$$

where the first term is Joule heating at tunnel junctions of resistance R_T, the second term is heat flow to phonons and P_0 accounts for parasitic heating. For a given phonon temperature, the minimum electron temperature T_e^{min} is found at $V_{DC} = 0$. If P_0 is small, then $T_e^{min} \approx T_p$.

Figure 2a shows the result of fitting the calculated $G(V_{DC})$ simultaneously to three measurements made between 20 and 60 mK. The fit parameters are R_T, C_Σ and T_P for each measurement. The fit is found to be insensitive to the value of P_0 and hence parasitic heating is assumed to be negligible at these temperatures. Having calibrated the CBT, the fitted C_Σ is used to fit further measurements with T_p and R_T as the free parameters. An example is given in Fig. 2a, where the electron temperature is found to be 7.2 ± 0.1 mK at a refrigerator temperature of 7.2 mK. Figure 2b shows that the electron temperature measured by the CBT is in close agreement with the refrigerator temperature T_{mxc} in both refrigerators between 7 and 80 mK. Details of how T_{mxc} was measured in each fridge can be found in the Methods section.

CBT characteristics below 7 mK. We investigate the behaviour of the CBT below 7 mK in the custom dilution refrigerator. Figure 3a shows the electron temperature of the sensor when in vacuum gradually cooling below 4 mK, while the refrigerator was held at $T_{mxc} \lessapprox 2.8$ mK. Here, T_e is determined from the value of G_0, which is found by measuring G over a small range of V_{DC} ($\approx 30\,\mu V$) close to $V_{DC} = 0$. We observe an extremely long equilibration time (over 3 days) but a rapid cooling of the CBT following a heating event (a refill of the liquid helium bath that briefly heats the CBT above 5.5 mK and the fridge above 3.5 mK). This suggests that the thermal contact between the CBT and the refrigerator is relatively strong, and that its slow cooling is probably due to heat leak from an external warm object.

A second CBT was immersed in the $^3He/^4He$ refrigerant of the custom dilution refrigerator to improve thermal coupling and better isolate external sources of heating. A schematic of the immersion cell is shown in the Fig. 3c. Sintered silver blocks increase the thermal contact between the refrigerant and the incoming contact wires[2]. Several sinters are attached to the sensor package, to each of the four measurement wires and to a grounding wire for the package and the *RC* filters. The immersed CBT is found to equilibrate much faster, as shown in Fig. 3a,

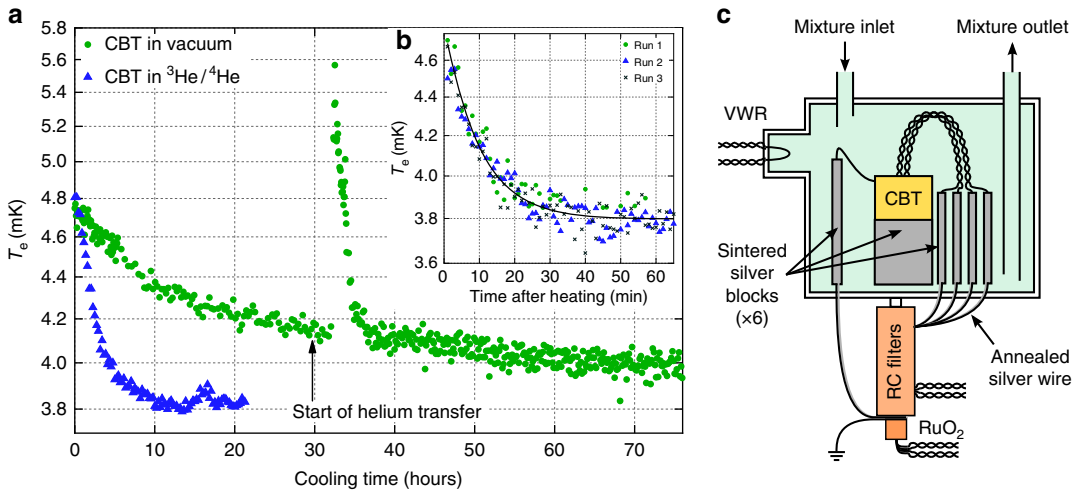

Figure 3 | Thermalization of two CBTs at a refrigerator temperature $\leq$ 2.8 mK. (**a**) Cooling of one CBT in vacuum (circles) and one immersed in the ^{3}He/^{4}He refrigerant of the dilution refrigerator (triangles). In both cases, the CBTs are cooling after being warmed above 10 mK by temporarily increasing the refrigerant temperature. The CBT in vacuum is extremely slow to thermalize. By comparison, the CBT immersed in ^{3}He/^{4}He thermalizes significantly faster. (**b**) Cooling of the immersed CBT after it has been heated by a large DC drive current (50, 40 and 30 nA for run 1, 2 and 3, respectively). Fitting to an exponential decay (solid line) yields a time constant of 570 s and a saturation temperature of 3.8 mK. (**c**) Schematic of the immersion cell used to cool a CBT in the ^{3}He/^{4}He mixture of a dilution refrigerator.

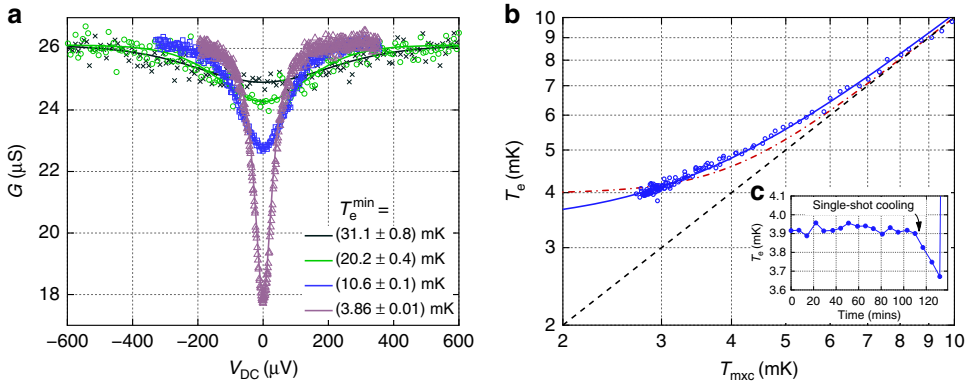

Figure 4 | Characteristics of a CBT immersed in ^{3}He/^{4}He refrigerant. (**a**) Fitting to the warmest three measurements gives $C_\Sigma = 209.5$ fF and $R_T = 23.21\,k\Omega$. The fitted minimum electron temperatures T_e^{min} for the warmest three curves are in reasonable agreement with the refrigerator temperatures as measured by the vibrating wire resonator (VWR) thermometer: 29.4, 19.0 and 10.5 mK, respectively. (**b**) Measured electron temperature in the CBT as the refrigerator cooled steadily from 10 to 2.7 mK over a period of 12 h. The solid curve shows a fit of the form $T_e^x = T_{mxc}^x + c$, yielding an exponent $x = 2.7$. The dot-dashed curve shows a best fit of $T_e^5 = T_{mxc}^5 + c$. The dashed line shows $T_e = T_{mxc}$. (**c**) The measured T_e as the refrigerator was temporarily cooled in single-shot mode to 2.2 mK, reaching a lowest T_e below 3.7 mK.

reaching $T_e \approx 3.8$ mK at $T_{mxc} \approx 2.7$ mK. It is important to note that even when T_e is elevated above T_p and T_{mxc}, the CBT remains a primary thermometer of its internal electron temperature.

To study the CBT at $|V_{DC}| > 0$, the time needed for the sensor to reach thermal equilibrium after a change of Joule heating needs to be known. Figure 3b shows the relaxation of T_e after the CBT has been heated by a large drive current for long enough to reach thermal equilibrium (>30 min). The subsequent value of T_e is measured by scanning close to $V_{DC} = 0$, where Joule heating should be negligible. The relaxation of T_e is found to have a time constant of 570 s.

Figure 4a shows the calibration of the immersed sensor. The three warmest measurements are fitted simultaneously to determine $C_\Sigma = 209.5$ fF and $R_T = 23.21\,k\Omega$. The fitted temperatures agree with T_{mxc} to within 6%. Given the agreement between the fitted T_e^{min} and T_{mxc}, we can assume that parasitic heating is still negligible down to 10 mK.

The coldest measurement in Fig. 4a is fitted using the above values, yielding a minimum electron temperature of 3.86 ± 0.01 mK. This measurement was made over a period of 7 h, to ensure that the CBT was in thermal equilibrium at each value of V_{DC}. At these temperatures, the parasitic heating of the CBT is now significant and T_e^{min} does not match the refrigerator temperature of $T_{mxc} = 2.7$ mK. To fit this conductance dip, the thermal model, equation 3, is used with $T_p = T_{mxc}$, and with the parasitic heating P_0 and the electron–phonon coupling $\Sigma\Omega$ as free parameters.

Figure 4b shows how the CBT electron temperature diverges from the refrigerator temperature below $\approx$7 mK. Here the value of T_e is found by measuring G_0 close to $V_{DC} = 0$ and so Joule heating can be neglected. The lowest temperature reported by the

CBT is below 3.7 mK when operating the fridge in single-shot mode (see Fig. 4c).

Discussion

The overheating of the sensor at $V_{DC}=0$ constrains the value of $P_0(\Sigma\Omega)^{-1}$ in the fit to the coldest measurement in Fig. 4a. However, the parasitic heating is not large enough to reliably separate the values of P_0 and $\Sigma\Omega$ in the fitting. Qualitatively, the fits suggest that $P_0 \geq 300$ aW per island and $\Sigma\Omega$ is at least four times larger than expected from the nominal size of the thermalization blocks and the literature value of Σ for Au[17]. It is not possible to determine an upper bound on P_0 without constraining $\Sigma\Omega$. It is worth noting that the power required to measure the CBT conductance ($\sim$1 aW per island due to Joule heating from I_{AC}) is much lower than our estimate of P_0. As such, we believe that CBTs of this type can be operated at still lower temperatures by further reducing the parasitic heating.

The functional form of T_e versus T_{mxc}, as shown in Fig. 4b, should have the same temperature dependence as the dominant thermalization mechanism, that is, T^5 for electron–phonon coupling. However, other power laws have been observed[9]. Here we find that the best fit of $T_e^x = T_{mxc}^x + c$ gives $x=2.7$ and a saturated T_e of $c^{1/x}=3.4$ mK. The fitted exponent x cannot be confirmed by fits to the conductance dips in Fig. 4a, because the overheating is still relatively weak, even at the lowest temperatures, and there is little effect on the shape of the dip. We find that a thermal model with a T^3 thermalization term fits the conductance dips equally well as a model using T^5.

The saturation of the measured CBT temperature below 7 mK could be caused by parasitic heating of the islands or excess voltage noise across the tunnel junctions. It is possible that the operating temperature could be lowered by reducing parasitic heating through better shielding and by lowering the voltage noise in the measurement circuit. To understand the cause of saturation in more detail, or to test an improved measurement environment, this sensor would need to be cooled closer to 1 mK.

In conclusion, the CBTs described here have been shown to operate as reliable primary thermometers of electron temperature down to 3.7 mK. The large thermalization blocks incorporated in the device and a relatively low level of parasitic heating ensure that the electron subsystem in the sensor is well coupled to the phonon subsystem down to $\approx$7 mK. An immersion cell is shown to improve thermal coupling between a CBT and a dilution refrigerator. This allows the onset of overheating to be observed below 7 mK, and although the presence of overheating can be seen, the effect is sufficiently weak that the sensor will need to be cooled further to fully characterize the thermalization mechanisms.

Methods

Device fabrication. The CBT devices are fabricated using an *ex situ* tunnel junction process[11]. The Al films that define the CBT circuit have a thickness of 250 nm. Tunnel junctions between sections of Al are formed by an insulating layer of 250 nm SiO_x deposited by plasma-enhanced chemical vapour deposition (PECVD). The junctions have a nominal diameter 0.8 μm and a resistivity $\sim$10 kΩ μm^2. The substrate is undoped Si with 300 nm thermal oxide on the surface.

The island thickness achievable with the *ex situ* tunnel junction process or other deposition techniques used for tunnel junction devices is typically up to 1 μm. Thicker films suffer from stress build-up, causing poor adhesion between the film and the substrate. This is a severe problem at mK temperatures where poor adhesion can lead to poor thermalization and even mechanical failure due to thermal motion during cool down. We avoid these problems by using a combination of the *ex situ* process followed by masked electroplating of Au on top of the CBT islands[22], which we refer to as thermalization blocks. Electroplating can produce $\sim$10 μm-thick, low-stress films and here we choose a nominal thickness of 5 μm for the thermalization blocks.

Refrigerator thermometry. Two different dilution refrigerators are used in the experiments described above. In the commercial refrigerator, the mixing chamber temperature T_{mxc} is measured by a calibrated RuO_2 resistor (Sensor model RU-1000-BF0.007 supplied and calibrated by Bluefors Cryogenics) in contact with the mixing chamber plate. In the custom refrigerator, T_{mxc} is measured using a conventional vibrating wire resonator viscometer immersed in the saturated dilute phase of the ^{3}He/^{4}He refrigerant in the mixing chamber[23,24]. The vibrating wire resonator is validated by comparison with a calibrated RuO_2 resistor (calibrated to 20 mK and supplied by Lake Shore Cryogenics). This resistor is thermally connected to the refrigerant via an immersed pad of sintered silver.

Data and software availability. All data used in this paper are available at http://dx.doi.org/10.17635/lancaster/researchdata/31, including descriptions of the data sets. The python-based pyCBT software library is freely available from Aivon Oy at https://github.com/AivonOy/pyCBT.

References

1. European Microkelvin Collaboration. EU-funded Integrating Activity project http://www.microkelvin.eu/ (2015).
2. Pan, W. *et al.* Exact quantization of the even-denominator fractional quantum Hall state at ν = 5/2 Landau level filling factor. *Phys. Rev. Lett.* **83,** 3530–3533 (1999).
3. Samkharadze, N. *et al.* Integrated electronic transport and thermometry at milliKelvin temperatures and in strong magnetic fields. *Rev. Sci. Instrum.* **82,** 053902 (2011).
4. Hanson, R., Kouwenhoven, L. P., Petta, J. R., Tarucha, S. & Vandersypen, L. M. K. Spins in few-electron quantum dots. *Rev. Mod. Phys.* **79,** 1217–1265 (2007).
5. Devoret, M. H. & Schoelkopf, R. J. Superconducting circuits for quantum information: an outlook. *Science* **339,** 1169–1174 (2013).
6. Giazotto, F., Heikkilä, T. T., Luukanen, A., Savin, A. M. & Pekola, J. P. Opportunities for mesoscopics in thermometry and refrigeration: physics and applications. *Rev. Mod. Phys.* **78,** 217–274 (2006).
7. Pekola, J. P., Hirvi, K. P., Kauppinen, J. P. & Paalanen, M. A. Thermometry by arrays of tunnel junctions. *Phys. Rev. Lett.* **73,** 2903–2906 (1994).
8. Meschke, M., Engert, J., Heyer, D. & Pekola, J. Comparison of Coulomb blockade thermometers with the international temperature scale PLTS-2000. *Int. J. Thermophys.* **32,** 1378–1386 (2011).
9. Casparis, L. *et al.* Metallic Coulomb blockade thermometry down to 10mK and below. *Rev. Sci. Instrum.* **83,** 083903 (2012).
10. Scheller, C. P. *et al.* Silver-epoxy microwave filters and thermalizers for millikelvin experiments. *Appl. Phys. Lett.* **104,** 211106 (2014).
11. Prunnila, M. *et al.* Ex situ tunnel junction process technique characterized by Coulomb blockade thermometry. *J. Vac. Sci. Technol. B* **28,** 1026–1029 (2010).
12. Hahtela, O. M. *et al.* Investigation of uncertainty components in Coulomb blockade thermometry. *AIP Conf. Proc.* **1552,** 142–147 (2013).
13. Gunnarsson, D. *et al.* Dielectric losses in multi-layer Josephson junction qubits. *Supercond. Sci. Technol.* **26,** 085010 (2013).
14. Meschke, M., Pekola, J., Gay, F., Rapp, R. & Godfrin, H. Electron thermalization in metallic islands probed by Coulomb blockade thermometry. *J. Low Temp. Phys.* **134,** 1119–1143 (2004).
15. Feshchenko, A. *et al.* Primary thermometry in the intermediate Coulomb blockade regime. *J. Low Temp. Phys.* **173,** 36–44 (2013).
16. Wellstood, F. C., Urbina, C. & Clarke, J. Hot-electron effects in metals. *Phys. Rev. B* **49,** 5942–5955 (1994).
17. Echternach, P. M., Thoman, M. R., Gould, C. M. & Bozler, H. M. Electron-phonon scattering rates in disordered metallic films below 1 K. *Phys. Rev. B* **46,** 10339–10344 (1992).
18. Roschier, L. *et al.* Effect of on-chip filter on Coulomb blockade thermometer. *J. Phys. Conf. Ser.* **400,** 052029 (2012).
19. Bladh, K. *et al.* Comparison of cryogenic filters for use in single electronics experiments. *Rev. Sci. Instrum.* **74,** 1323–1327 (2003).
20. Bradley, D. I., Follows, M., Miller, I., Oswald, R. & Ward, M. Simple design for dilution refrigerator with base temperature of 2.3mK. *Cryogenics* **34,** 549–550 (1994).
21. Farhangfar, S. *et al.* One dimensional arrays and solitary tunnel junctions in the weak Coulomb blockade regime: CBT thermometry. *J. Low Temp. Phys.* **108,** 191–215 (1997).
22. Xu, H. *et al.* Wafer-level SLID bonding for MEMS encapsulation. *Adv. Manuf.* **1,** 226–235 (2013).
23. Zeegers, J., de Waele, A. & Gijsman, H. Viscosity of saturated ^{3}He-^{4}He mixture below 200 mK. *J. Low Temp. Phys.* **84,** 37–47 (1991).
24. Pentti, E., Rysti, J., Salmela, A., Sebedash, A. & Tuoriniemi, J. Studies on helium liquids by vibrating wires and quartz tuning forks. *J. Low Temp. Phys.* **165,** 132–165 (2011).

Acknowledgements

We thank Jukka Pekola and Matthias Meschke for useful discussions, and Andrey Shchepetov for producing the scanning electron microscopic images in Fig. 1. This research is supported by the U.K. EPSRC (EP/K01675X/1 and EP/L000016/1), the European FP7 Programme MICROKELVIN (project number 228464), Tekes project FinCryo (grant number 220/31/2010), Academy of Finland (project number 252598) and the Royal Society. J.R.P. acknowledges support of the People Programme (Marie Curie Actions) of the European FP7 Programme under REA grant agreement 618450. Yu.A.P. acknowledges support by the Royal Society and the Wolfson Foundation.

Author contributions

D.G., H.H., J.P., M.P. and L.R. designed, fabricated and packaged the devices. J.P. and L.R. developed custom measurement instrumentation and methods. D.I.B., R.E.G., R.P.H., Yu.A.P., J.R.P., L.R. and M.S. performed measurements and calculations. J.R.P. drafted the manuscript. All authors discussed the results and implications, and commented on the manuscript at all stages.

Additional information

Competing financial interests: The authors declare no competing financial interests.

Reprints and permission information is available online at http://npg.nature.com/reprintsandpermissions/

How to cite this article: Bradley, D. I. *et al.* Nanoelectronic primary thermometry below 4 mK. *Nat. Commun.* 7:10455 doi: 10.1038/ncomms10455 (2016).

nature COMMUNICATIONS

DOI: 10.1038/ncomms11678 OPEN

Erratum: Nanoelectronic primary thermometry below 4 mK

D.I. Bradley, R.E. George, D. Gunnarsson, R.P. Haley, H. Heikkinen, Yu A. Pashkin, J. Penttilä, J.R. Prance, M. Prunnila, L. Roschier & M. Sarsby

Nature Communications 7:10455 doi: 10.1038/ncomms10455 (2016); Published 27 Jan 2016; Updated 3 Jun 2016

The affiliation details for L. Roschier are incorrect in this Article. The correct affiliation details for this author are given below:

Aivon Oy, Valimotie 13A, 00380 Helsinki, Finland.